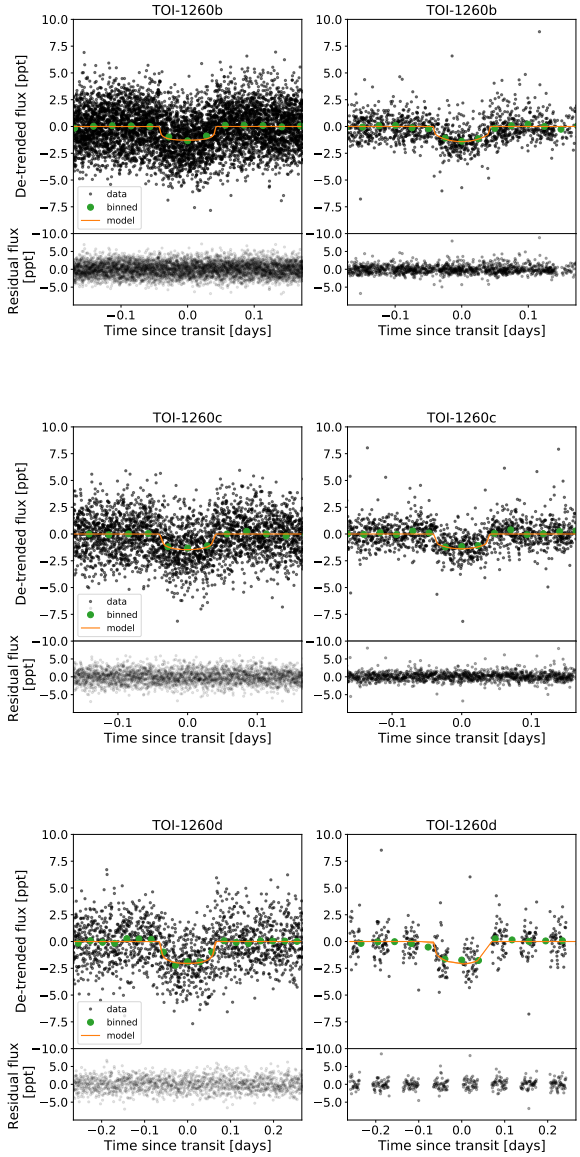

Figure 2. Phase folded light curves of TOI-1260b (top), TOI-1260c (middle), TOI-1260d (bottom). The TESS data are shown in the left panels and the CHEOPS data are shown in the right panels. Residuals of each transit are shown below each phase-folded light curves. The phase binned data are denoted by green points and the orange line shows the best-fitted transit models for each planet.

mass determination of planets b and c are consistent within 1-sigma with values derived in G21.

The mass precision of the planets is the main source of uncertainty in the determination of the planetary bulk densities in the system. This work highlights the need to strategically obtain more RVs for the system in order to understand the effect of stellar activity on the RVs of the system and better constrain the planetary masses.

6 DISCUSSION

The follow-up photometric observations of TOI-1260 allows the precise characterisation of the two inner transiting planets and confirms the planetary nature of the transiting outer planetary companion. Figure 5 shows the mass-radius diagram of known exoplanets with masses below 30 $M_\oplus$ and radii less than 4 $R_\oplus$. We proceed now with the discussion of the interior composition and atmospheric evolution of the planetary system.

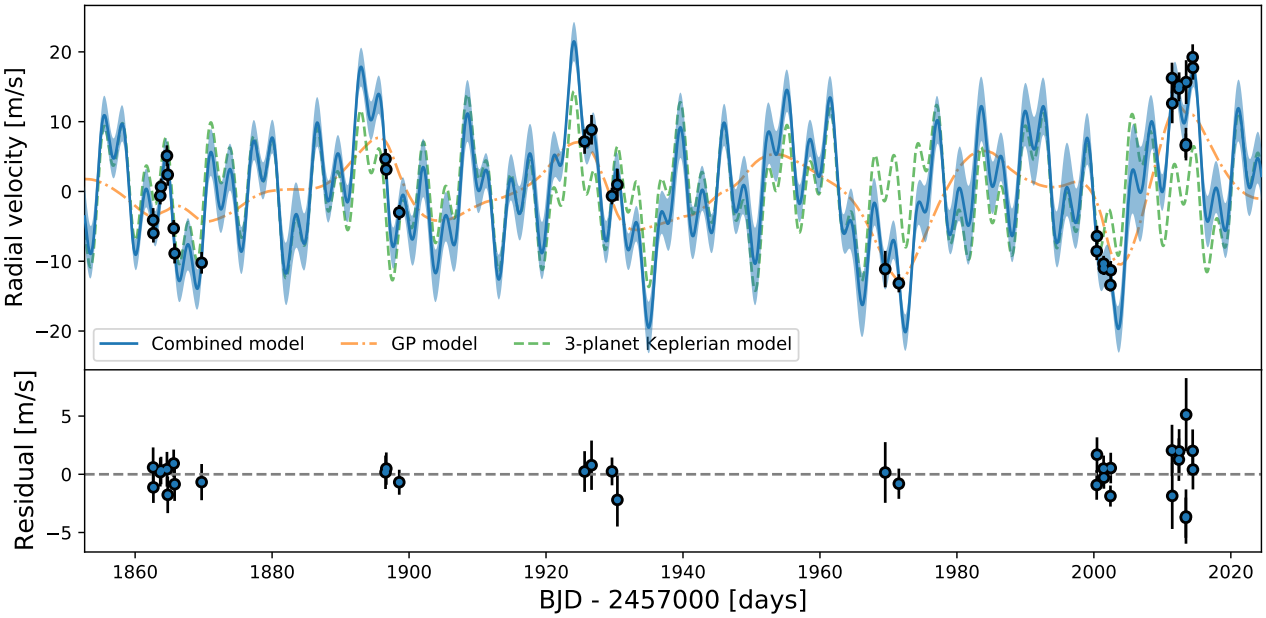

Figure 3. *Top:* Time-series HARPS-N RVs of TOI-1260. The RVs were modelled using a three-planet Keplerian RV model and a GP simultaneously to model the activity-induced RV variations (see Section 5). The green dash line shows the 3-planet Keplerian model and the orange dash-dot line shows the GP model that accounts for activity induced RV variations. The blue solid line shows the median three-planet Keplerian + GP model. The 1-sigma credible intervals of the best fit Keplerian + GP model is indicated by the blue shaded region.

Bottom: Residuals of the RV data.

Table 3. System parameters obtained from the joint light curves and radial velocities analysis. The median values and 1-sigma uncertainty are reported.

Parameter [Unit]	Planet b	Planet c	Planet d
Fitted parameters			
Period P [day]	3.127463 ± 0.000005	7.493134 ± 0.000020	16.608164 ± 0.000083
Epoch T0 [BJD-2457000]	2065.564269 ± 0.000396	2068.270505 ± 0.000577	2062.017406 ± 0.001309
Planet-to-Stellar radius ratio [Rp/Rs]	0.0329 ± 0.0006	0.0377 ± 0.0007	0.0425 ± 0.0009
Impact paramater b	0.20 ± 0.12	0.75 ± 0.02	0.53 ± 0.05
Radial velocity semi-amplitude K [m s^{-1}]	4.93 ± 0.83	5.67 ± 1.77	3.90 ± 2.54
Eccentricity e	0 (adopted)	0 (adopted)	0 (adopted)
Angle of periastron ω [°]	0 (adopted)	0 (adopted)	0 (adopted)
Derived parameters			
Transit duration T14 [hr]	2.06 ± 0.02	1.97 ± 0.03	3.19 ± 0.07
Transit depth [ppm]	1082 ± 37	1421 ± 55	1808 ± 78
Scaled semi-major axis a/Rs	11.73 ± 0.35	20.99 ± 0.63	35.69 ± 1.06
Orbital semi-major axis a [au]	0.0367 ± 0.0011	0.0657 ± 0.0020	0.1116 ± 0.0033
Inclination i [deg]	89.03 ± 0.61	87.97 ± 0.11	89.14 ± 0.10
Planet radius R_p [$R_\oplus$]	2.41 ± 0.05	2.76 ± 0.07	3.12 ± 0.08
Planet mass M_p [$M_\oplus$]	8.56 ± 1.54	13.20 ± 4.23	11.84 ± 7.79
Planet density ρ_p [$g\ cm^{-3}$]	3.35 ± 0.64	3.45 ± 1.14	2.14 ± 1.42
Planet surface gravity log g_p	3.16 ± 0.09	3.23 ± 0.15	3.08 ± 0.30
Equilibrium dayside temperature [K]	871 ± 24	651 ± 18	499 ± 14
Stellar insolation [$S_\oplus$]	95.58 ± 0.07	29.81 ± 0.05	10.32 ± 0.07
TESS instrument offset $\sigma_{\rm TESS}$ [ppm]	64.0 ± 8.6		
CHEOPS instrument offset $\sigma_{\rm TESS}$ [ppm]	48.8 ± 14.7		
HARPS jitter $\sigma_{\rm HARPS}$ [m s^{-1}]	0.22 + /−0.79		
Systemic radial velocity $\gamma_{\rm HARPS}$ [m s^{-1}]	10.73 ± 2.63		
Limb darking parameter $u_{1,\rm TESS}$	0.21 ± 0.18		
Limb darkening parameter $u_{2,\rm TESS}$	0.53 ± 0.26		
Limb darking parameter $u_{1,\rm CHEOPS}$	0.92 ± 0.18		
Limb darking parameter $u_{2,\rm CHEOPS}$	−0.33 ± 0.21		
GP `RotationTerm` *parameters*			
GP rotation period $R_{\rm rot,GP}$ [day]	30.63 ± 3.81		
$\sigma_{\rm GP}$	6.62 ± 1.45		
$Q0$	0.83 ± 1.48		
dQ	1.94 ± 3.67		
f	0.70 ± 0.23		
Stellar mass $M_{\rm s}$ [$M_\odot$]	0.67 ± 0.06		
Stellar radius $R_{\rm s}$ [$R_\odot$]	0.67 ± 0.01		
Stellar density $\rho_{\rm s}$ [g cm^{-3}]	3.12 ± 0.33		

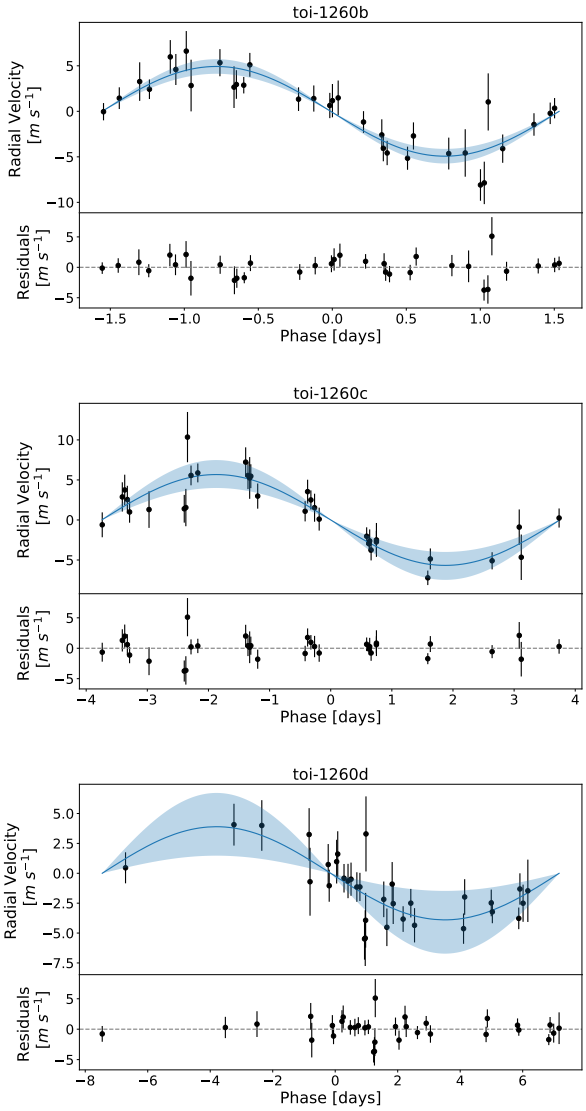

Figure 4. Phase-folded radial velocities and residuals of TOI-1260b (top), TOI-1260c (middle), TOI-1260d (bottom). The best-fit RV models are indicated by the solid blue line and the corresponding 1-sigma credible interval is shown by the blue shaded region.

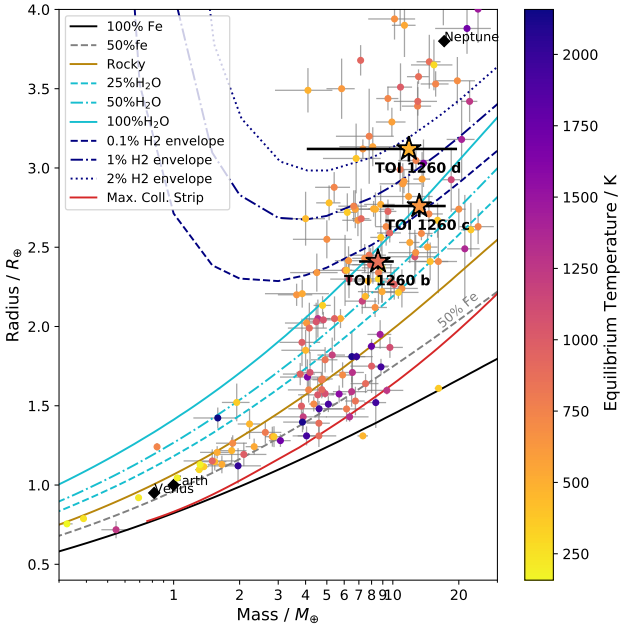

Figure 5. Mass-radius diagram showing low mass planets in the range of 0.4-30 $M_\oplus$ which have mass and radius precision measured to better than 30% and 15%, respectively. TOI-1260b, TOI-1260c, TOI-1260d, are indicated by the star symbols. All exoplanets are colour-coded according to their the equilibrium dayside temperatures as shown in the colour bar. The different lines plotted are the theoretical mass-radius relations corresponding to the planet interior compositions (Zeng et al. 2019).

6.1 Interior composition of the planets

The TOI-1260 system has three sub-Neptune transiting exoplanets where planets b, c and d have masses of $8.56 \pm 1.54\ M_\oplus$, $13.20 \pm 4.23\ M_\oplus$ and $11.84 \pm 7.79\ M_\oplus$, respectively, and their radii are $2.41 \pm 0.05\ R_\oplus$, $2.76 \pm 0.07\ R_\oplus$, and $3.12 \pm 0.08\ R_\oplus$, respectively. This means that the three sub-Neptunes TOI-1260 b, c and d have bulk densities of 3.35 ± 0.64 g cm^{-3}, 3.45 ± 1.14 g cm^{-3}, and 2.14 ± 1.42 g cm^{-3}, respectively. Figure 5 shows the distribution of known exoplanet with precise mass and radius measurements in the mass-radius diagram, alongside some theoretical mass-radius relations for different planet interior compositions. The interior of TOI-1260 b is likely to be consisted of up up 50% rocky core and a 50% H_2O layer. In the case of TOI-1260 c, the sub-Neptune planet is likely a water world or it could be composed of a water-rich core with a small fraction of H2 atmosphere. For the outermost planet TOI-1260 d, its interior is likely to consist of a water-rich or Earth-like rocky core with up to $\sim 2\%$ of H2 atmosphere.

The interior compositions of exoplanet correlates with the compositions of their host stars (Adibekyan et al. 2021a). This is because they were formed from accretion of the same disk material. Therefore, using physical parameters of the host star in addition to the planet's mass and radius provides a better constrain to the planet's interior composition. Using the values of radius, mass, and stellar properties derived in Section 5, we performed an analysis of the internal structure of the three planets in the TOI-1260 system. Our method is based on a global Bayesian model that fits the observed properties of the star (mass, radius, age, effective temperature, and the photospheric abundances [Si/Fe] and [Mg/Fe]) and planets (planet-star radius ratio, the RV semi-amplitude, and the orbital period). The hidden parameters in the Bayesian model are, for each planet, the masses of solids (everything except the H or He gas), the mass fractions of the core, mantle and water, the mass of the gas envelope, the Si/Fe and Mg/Fe mole ratios in the planetary mantle, the S/Fe mole ratio in the core, and the equilibrium temperature. All details on the methods are presented in Leleu et al. (2021).

The Bayesian analysis relies on a forward models that computes the expected planetary radius and bulk internal structure as a function of the hidden parameters. In the forward model, we assume a fully differentiated planet made of a core (composed of Fe and S), a mantle (composed of Si, Mg, Fe, and O), a pure water layer, and a H and He layer. The temperature profile is adiabatic, and the equations of state (EoS) used for these calculations are taken from Hakim et al. (2018) and Fei et al. (2016) for the core materials, from Sotin et al. (2007) for the mantle materials, and Haldemann et al. (2020) for water. The thickness of the gas envelope is determined as a function of the gas mass fraction, the equilibrium temperature, the mass and radius of the solid planet, and the age (assumed to be equal to the stellar age), using the semi-analytical model of Lopez & Fortney (2014). Importantly, the radius of the high-Z part of the planet (core, mantle and water layer) is computed independently of the thickness of the gas layer. This implies in particular that the compression effect of the gas envelope onto the core, as well as the effect of the temperature at the basis of the gas envelope are not included in the mode.

The Bayesian analysis is done assuming the following priors: the mass fractions of the planetary cores, mantles, and water layers have uniform positive priors (the mass fractions of water being limited to a maximum value of 0.5). The prior on the gas mass is uniform in log, and the bulk Si/Fe and Mg/Fe mole ratios in the planet are assumed to be equal to the values determined for the atmosphere of the star, given above [3].

The posterior distribution of the main planetary hidden parameters are presented in Fig. 6. All planets have some fraction of gas, the mass of gas increasing for decreasing equilibrium temperatures (see Fig. 7). The fraction of water, on the other hand, is essentially unconstrained.

6.2 Atmospheric evolution

We considered the stellar and planetary parameters derived in our paper, as well as the present-day planetary atmospheric mass fractions presented in Section 6.1, to reconstruct the evolution of the stellar rotation rate and of the planetary atmospheres. In particular, we constrain the evolution of the stellar rotation period, which we use as proxy for the evolution of the stellar high-energy emission affecting atmospheric escape, and the predicted initial atmospheric mass fraction of the detected planets $f_{\rm atm}^{\rm start}$, that is the mass of the planetary atmosphere at the time of the dispersal of the protoplanetary disk, which we assume being at 5 Myr.

We reach these results by using the *P*lanetary *A*tmospheres and *S*tellar Ro*T*ation R*A*tes (PASTA; Bonfanti et al. 2021b) code, which is an updated version of the original code presented by Kubyshkina et al. (2019c,a). In short, PASTA constraints the evolution of planetary atmospheres and of the stellar rotation rate combining a model predicting planetary atmospheric escape rates based on hydrodynamic simulations (this has the advantage over other commonly used analytical estimates to account for both XUV-driven and core-powered mass loss; Kubyshkina et al. 2018), a model of the stellar high-energy (X-ray plus extreme ultraviolet; XUV) flux evolution (Bonfanti et al. 2021b), a model relating planetary parameters and atmospheric mass (Johnstone et al. 2015b), and stellar evolutionary tracks (Choi et al. 2016). PASTA works under two main assumptions: 1) planet migration did not occur after the dispersal of the protoplanetary disk; 2) the planets hosted at some point in the past or still host a hydrogen-dominated atmosphere. PASTA returns realistic uncertainties on the free parameters (i.e. the planetary initial atmospheric mass fractions at the time of the dispersal of the protoplanetary disk, and the indexes of the power law controlling the stellar rotation period that is used as proxy for the stellar XUV emission) by implementing the atmospheric evolution algorithm in a Bayesian framework (Cubillos et al. 2017), using the system parameters with their uncertainties as input priors. All details of the algorithm can be found in Bonfanti et al. (2021b). The only difference with respect to the analysis of the systems considered by Bonfanti et al. (2021b) is that here we fit the planetary atmospheric mass fractions given in Section 6.1 instead of the planetary radii. This enables the code to be more accurate by avoiding the continuous conversion of the atmospheric mass fraction into planetary radius, given the other system parameters (see e.g. Delrez et al. 2021).

Figure 8 shows the results obtained from PASTA. As a proxy for the evolution of the stellar rotation period, Figure 8 displays the posterior distribution of the stellar rotation period at an age of 150 Myr ($P_{\rm rot,150}$), also in comparison to that of stars member of young open clusters and of comparable mass extracted from Johnstone et al. (2015a). The posterior distribution is slightly shifted towards slower rotation compared to that of the open cluster stars, indicating that the

[3] It should be noted however that Adibekyan et al. (2021b) has found that despite an existing correlation between the abundances of planets and host stars, the relation is not always strictly one-to-one.

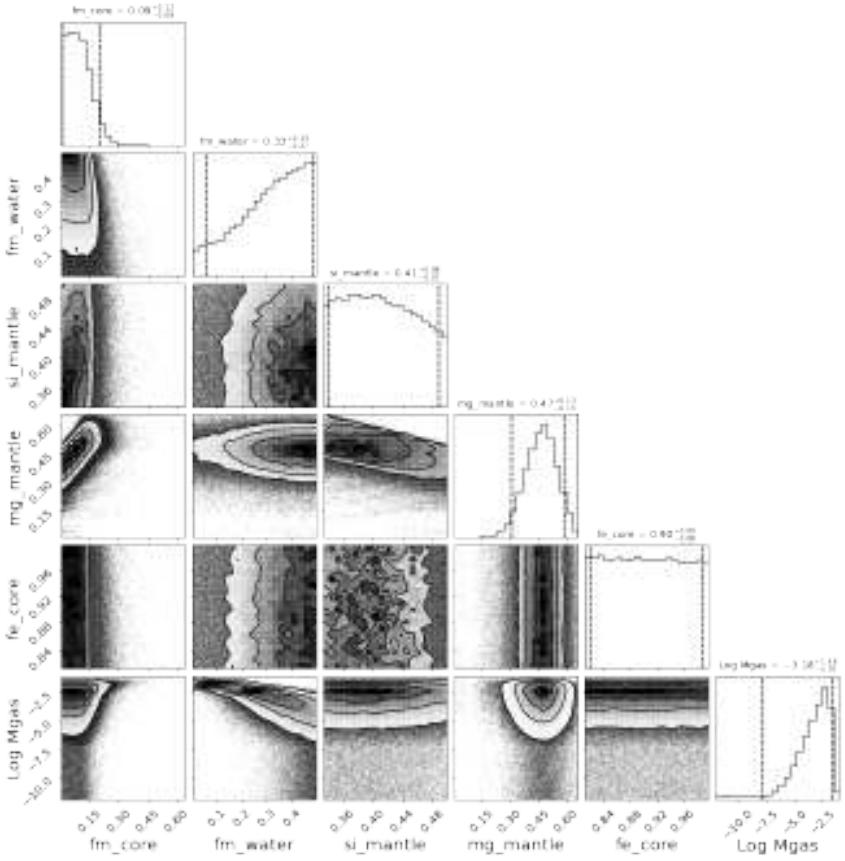
fm_core
fm_water
si_mantle
mg_mantle
fe_core
Log Mgas

(a)

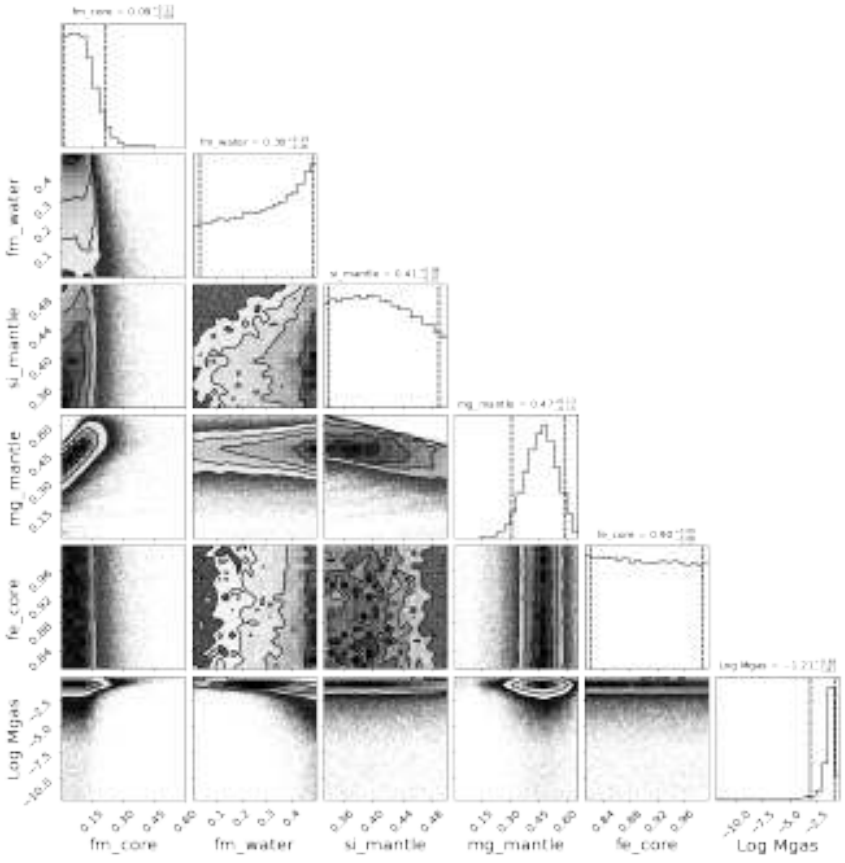
fm_core
fm_water
si_mantle
mg_mantle
fe_core
Log Mgas

(b)

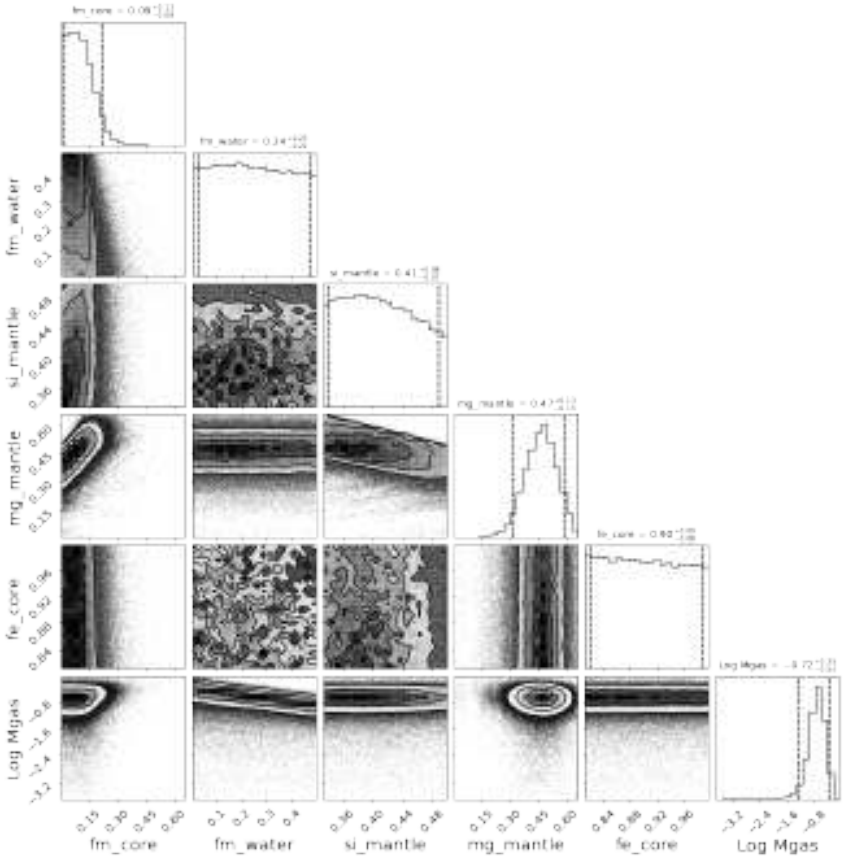

(c)

Figure 6. Corner plot showing the results on the interior composition models of (a) TOI-1260 b, (b) TOI-1260 c and (c) TOI-1260 d. The vertical dashed lines and the 'error bars' given at the top of each columns represent the 5 % and 95 % percentiles.

planets were likely subject to somewhat less XUV radiation than the average.

Figure 8 shows also the posterior distribution of the initial atmospheric mass fraction for planets b (in linear scale), c (in logarithmic scale), and d (in logarithmic scale) in comparison to the present-day atmospheric mass fraction (Section 6.1). The posterior distribution for planet b is flat, indicating that the planet has most likely lost (almost) entirely its primordial hydrogen-dominated envelope through escape at some point in the past, which is why PASTA is unable to constrain the initial atmospheric mass fraction. Figure 8 indicates that also planets c and d have gone through significant evolution through escape that has significantly eroded the primordial atmospheric content, which was however small in comparison to the planetary masses. Therefore, we conclude that both planets (i.e. c and d) accreted a small hydrogen envelope during the formation process compared to their masses. This may have been the result of several physical mechanisms, such as late planet formation compared to the age of the protoplanetary disk, early dispersal of the protoplanetary disk, low gas content of the disk.

As the isochronal age is loosely constrained, we performed additional evolution runs by artificially making the star much younger or older, further imposing tighter constraints on the stellar age. Despite the different evolutionary time scales, we did not find significant changes in the $f_{\rm atm}^{\rm start}$ of the planets. This is because (1) atmospheric mass loss is significant only during the first Myrs of evolution and (2) $f_{\rm atm,c}^{\rm start}$ and $f_{\rm atm,d}^{\rm start}$ are always found to be rather small, indicating that the constraints given by system parameters prevent those planets to host a massive initial atmosphere regardless of the age of the system.

The current stellar XUV fluxes impinging on each planet are $F_{\rm XUV,b} = 2.87 \cdot 10^4$ erg/(cm^2 s), $F_{\rm XUV,c} = 8.97 \cdot 10^3$ erg/(cm^2 s), and $F_{\rm XUV,d} = 3.10 \cdot 10^3$ erg/(cm^2 s). The correspondent mass-loss rate values expected for the planets right now are $\dot{M}_b = 10^{10}$ g/s, $\dot{M}_c = 1.59 \cdot 10^9$ g/s, and $\dot{M}_d = 7.43 \cdot 10^8$ g/s. Assuming that the stellar XUV flux does not change over time in the future, which is a reasonable assumption given the old age of the star, these values imply that in the next Gyr the planets are respectively going to lose 0.6%, 0.06%, and 0.03% of their mass. From Fig. 7 these values then imply that planet b is going to lose entirely its hydrogen-dominated envelope, while planets c and d are going to keep it. As the results of planet b are consistent with no hydrogen atmosphere at all, it is unlikely that the position of these planets in the period-radius diagram (e.g. Fulton et al. 2017) is going to change in the future.

7 CONCLUSIONS

We presented the follow-up observations of the TOI-1260 system using CHEOPS and TESS. The addition of the recent photometric dataset allow us to refine the physical parameters of the planetary system and discover a third additional transiting planet. For planets TOI-1260 b and c, we found that the radii are 2.36 ± 0.06 R$_\oplus$, 2.82 ± 0.08 R$_\oplus$, respectively, and the masses 8.52 ± 1.45 M$_\oplus$ and $13.29 \pm$

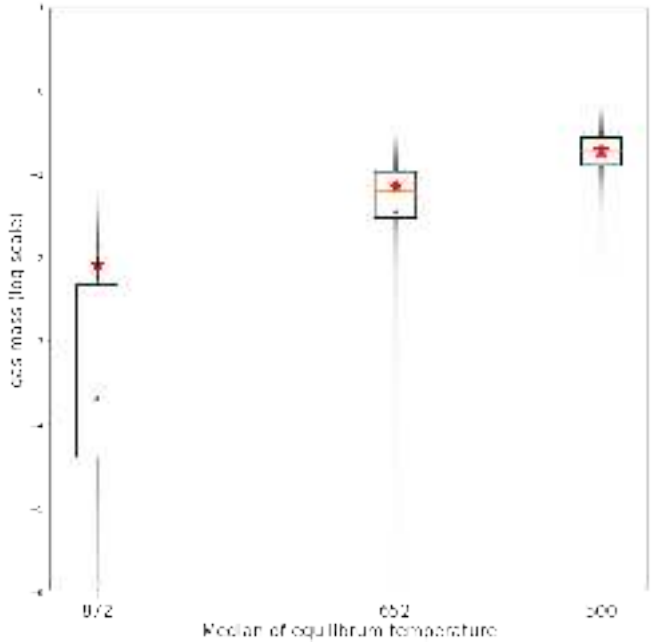

Figure 7. Gas fraction in the planets as a function of their equilibrium temperature. The box show the 25 % and 75 % percentiles, the orange line represents the median of the posterior distribution, the green triangle is the mean, and the red stars is located at the mode of the posterior distribution. Finally, the opacity of the thick vertical black line is proportional to the posterior distribution.

3.94 $M_\oplus$. The newly discovered TOI-1260-d has bulk properties 3.01 ± 0.09 $R_\oplus$ and 11.8 ± 7.5 $M_\oplus$.

The detailed characterization of the planetary parameters allows us to derive constraints of their internal composition and evolution that we related to the formation processes in the system and its future evolution.

The TOI-1260 system presents an exciting opportunity for comparative exoplanetology using JWST transmission spectroscopy. Moses et al. (2013) predicted that sub-Neptune sized exoplanets such as those in the TOI-1260 system can harbour a large diversity of atmospheric compositions. Multi-planet systems such as TOI-1260 give us the opportunity to test whether such diversity can exist within different sub-Neptunes in the same system. All three of the planets in the TOI-1260 system appear to be favourable for atmospheric categorisation with JWST, with transmission spectroscopy metrics (TSMs Kempton et al. 2018) of 43.6, 36.1 and 40.4 for planets b, c, and d, respectively. Figure 9 shows how this compares to similar multi-planet systems as a function of planetary radius and semi-major axis. In addition, due to its high northern declination TOI-1260 is particularly favourable for JWST visibility, with observations possible for 196 days each year (Bourque et al. 2021).

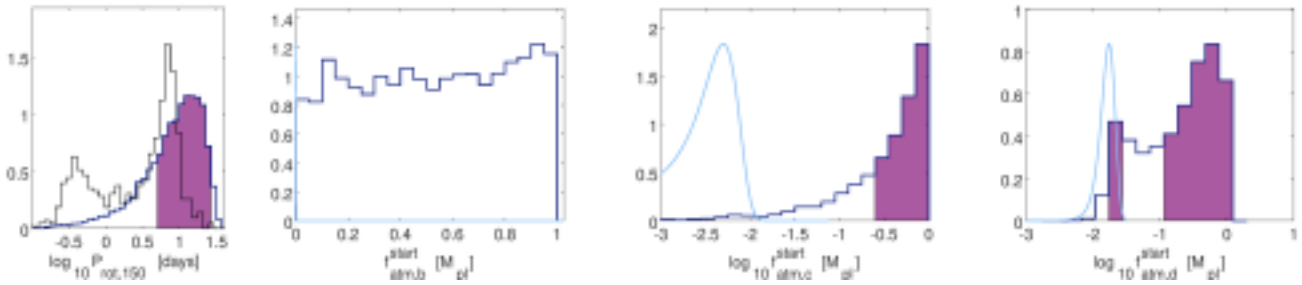

Figure 8. Posterior probability density functions (PDFs) of the stellar rotation period when TOI-1260 was 150 Myr old ($P_{\rm rot,150}$) and of the initial atmospheric mass fraction ($f_{\rm atm}^{\rm start}$) of the hosted exoplanets. The purple areas show the 68%-HPD (highest posterior density) interval. *Leftmost panel.* $P_{\rm rot,150}$ PDF (dark blue histogram) to be compared with the rotation period distribution of stars of comparable masses that belong to coeval open clusters (black histogram; data taken from Johnstone et al. 2015a). *Other panels.* Atmospheric mass fractions PDFs of planet b (linear scale) and of planet c and d (log scale). The light blue curve is the present-day atmospheric content, as inferred from our internal structure analysis. See text for details.

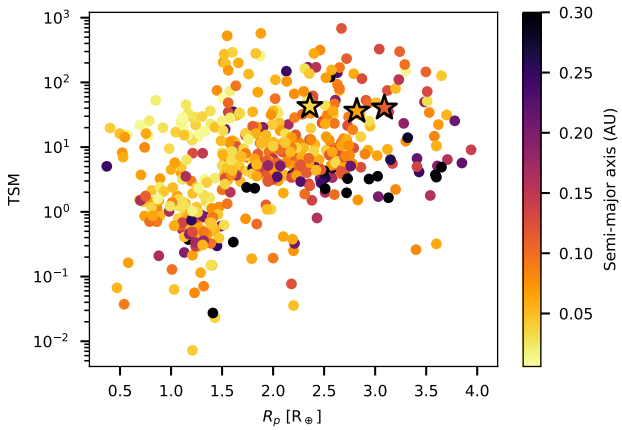

Figure 9. Unscaled transmission spectroscopy metrics (TSM) of all multi-planet systems with host stars of K-type and later as a function of planetary radius, with orbital separation visible in the colour scale. The three planets in the TOI-1260 system are marked with stars.

ACKNOWLEDGEMENTS

CHEOPS is an ESA mission in partnership with Switzerland with important contributions to the payload and the ground segment from Austria, Belgium, France, Germany, Hungary, Italy, Portugal, Spain, Sweden, and the United Kingdom. The CHEOPS Consortium would like to gratefully acknowledge the support received by all the agencies, offices, universities, and industries involved. Their flexibility and willingness to explore new approaches were essential to the success of this mission.

KGI is the ESA CHEOPS Project Scientist and is responsible for the ESA CHEOPS Guest Observers Programme. She does not participate in, or contribute to, the definition of the Guaranteed Time Programme of the CHEOPS mission through which observations described in this paper have been taken, nor to any aspect of target selection for the programme.

K.W.F.L. acknowledge support by DFG grants RA714/14-1 within the DFG Schwerpunkt SPP 1992, “Exploring the Diversity of Extrasolar Planets”.

YA, MJH and JAE acknowledge the support of the Swiss National Fund under grant 200020_172746.

CMP, MF and IYG gratefully acknowledge the support of the Swedish National Space Agency (DNR 65/19, 174/19, 174/18).

SH gratefully acknowledges CNES funding through the grant 837319.

ACC and TW acknowledge support from STFC consolidated grant numbers ST/R000824/1 and ST/V000861/1, and UKSA grant number ST/R003203/1.

We acknowledge support from the Spanish Ministry of Science and Innovation and the European Regional Development Fund through grants ESP2016-80435-C2-1-R, ESP2016-80435-C2-2-R, PGC2018-098153-B-C33, PGC2018-098153-B-C31, ESP2017-87676-C5-1-R, MDM-2017-0737 Unidad de Excelencia ”María de Maeztu”- Centro de Astrobiolog’ia (INTA-CSIC), as well as the support of the Generalitat de Catalunya/CERCA programme. The MOC activities have been supported by the ESA contract No. 4000124370.

S.C.C.B. acknowledges support from FCT through FCT contracts nr. IF/01312/2014/CP1215/CT0004.

XB, SC, DG, MF and JL acknowledge their role as ESA-appointed CHEOPS science team members.

ABr was supported by the SNSA.

This project was supported by the CNES.

LD is an F.R.S.-FNRS Postdoctoral Researcher. The Belgian participation to CHEOPS has been supported by the Belgian Federal Science Policy Office (BELSPO) in the framework of the PRODEX Program, and by the University of Liège through an ARC grant for Concerted Research Actions financed by the Wallonia-Brussels Federation.

This work was supported by FCT - Fundação para a Ciência e a Tecnologia through national funds and by FEDER through COMPETE2020 - Programa Operacional Competitividade e Internacionalização by these grants: UID/FIS/04434/2019; UIDB/04434/2020; UIDP/04434/2020; PTDC/FIS-AST/32113/2017 & POCI-01-0145-FEDER-032113; PTDC/FIS-AST/28953/2017 & POCI-01-0145-FEDER-028953; PTDC/FIS-AST/28987/2017 & POCI-01-0145-FEDER-028987. O.D.S.D. is supported in the form of work contract (DL 57/2016/CP1364/CT0004) funded by national funds through FCT.

B.-O.D. acknowledges support from the Swiss National Science Foundation (PP00P2-190080).

This project has received funding from the European Research Council (ERC) under the European Union’s Horizon 2020 research and innovation programme (project Four Aces; grant agreement No 724427). It has also been carried out in the frame of the National Centre for Competence in Research PlanetS supported by the Swiss National Science Foundation (SNSF). DE acknowledges financial support from the Swiss National Science Foundation for project 200021_200726.

DG gratefully acknowledges financial support from the CRT foundation under Grant No. 2018.2323 "Gaseousor rocky? Unveiling the nature of small worlds".
M.G. is an F.R.S.-FNRS Senior Research Associate.
This work was granted access to the HPC resources of MesoPSL financed by the Region Ile de France and the project Equip@Meso (reference ANR-10-EQPX-29-01) of the programme Investissements d'Avenir supervised by the Agence Nationale pour la Recherche.
ML acknowledges support of the Swiss National Science Foundation under grant number PCEFP2_194576.
GSc, GPi, IPa, LBo, VNa and RRa acknowledge the funding support from Italian Space Agency (ASI) regulated by "Accordo ASI-INAF n. 2013-016-R.0 del 9 luglio 2013 e integrazione del 9 luglio 2015 CHEOPS Fasi A/B/C".
PM acknowledges support from STFC research grant number ST/M001040/1.
This work was also partially supported by a grant from the Simons Foundation (PI Queloz, grant number 327127).
IR acknowledges support from the Spanish Ministry of Science and Innovation and the European Regional Development Fund through grant PGC2018-098153-B- C33, as well as the support of the Generalitat de Catalunya/CERCA programme.
S.G.S. acknowledge support from FCT through FCT contract nr. CEECIND/00826/2018 and POPH/FSE (EC).
GyMSz acknowledges the support of the Hungarian National Research, Development and Innovation Office (NKFIH) grant K-125015, a PRODEX Institute Agreement between the ELTE Eötvös Loránd University and the European Space Agency (ESA-D/SCI-LE-2021-0025), the Lendület LP2018-7/2021 grant of the Hungarian Academy of Science and the support of the city of Szombathely.
V.V.G. is an F.R.S-FNRS Research Associate.
S.S. has received funding from the European Research Council (ERC) under the European Union's Horizon 2020 research and innovation programme (grant agreement No 833925, project STAREX). R.L. acknowledges funding from University of La Laguna through the Margarita Salas Fellowship from the Spanish Ministry of Universities ref. UNI/551/2021-May 26, and under the EU Next Generation funds. This paper includes data collected with the TESS mission, obtained from the MAST data archive at the Space Telescope Science Institute (STScI). Funding for the TESS mission was provided by the NASA Explorer Program. STScI is operated by the Association of Universities for Research in Astronomy, Inc., under NASA contract NAS 5–26555.

DATA AVAILABILITY

TESS data are publicly available in the Space Telescope Science Institute (STScI) at https://mast.stsci.edu. CHEOPS data generated and analysed in this article will be made available in the CHEOPS mission archive (https://cheops.unige.ch/archive_browser/). No new HARPS RV data were generated for this work.

REFERENCES

Adibekyan V., et al., 2021a, Science, 374, 330
Adibekyan V., et al., 2021b, Science, 374, 330
Armstrong D. J., et al., 2020, Nature, 583, 39
Benz W., et al., 2021, Experimental Astronomy, 51, 109
Blackwell D. E., Shallis M. J., 1977, MNRAS, 180, 177
Bonfanti A., Ortolani S., Piotto G., Nascimbeni V., 2015, A&A, 575, A18
Bonfanti A., Ortolani S., Nascimbeni V., 2016, A&A, 585, A5
Bonfanti A., et al., 2021a, A&A, 646, A157
Bonfanti A., Fossati L., Kubyshkina D., Cubillos P. E., 2021b, A&A, 656, A157
Borucki W. J., et al., 2010, Science, 327, 977
Bourque M., et al., 2021, The Exoplanet Characterization Toolkit (ExoCTK), doi:10.5281/zenodo.4556063
Castelli F., Kurucz R. L., 2003, in Piskunov N., Weiss W. W., Gray D. F., eds, IAU Symposium Vol. 210, Modelling of Stellar Atmospheres. p. A20 (arXiv:astro-ph/0405087)
Choi J., Dotter A., Conroy C., Cantiello M., Paxton B., Johnson B. D., 2016, ApJ, 823, 102
Cosentino R., et al., 2012, in McLean I. S., Ramsay S. K., Takami H., eds, Society of Photo-Optical Instrumentation Engineers (SPIE) Conference Series Vol. 8446, Ground-based and Airborne Instrumentation for Astronomy IV. p. 84461V, doi:10.1117/12.925738
Cosentino R., et al., 2014, in Ramsay S. K., McLean I. S., Takami H., eds, Society of Photo-Optical Instrumentation Engineers (SPIE) Conference Series Vol. 9147, Ground-based and Airborne Instrumentation for Astronomy V. p. 91478C, doi:10.1117/12.2055813
Cubillos P., Harrington J., Loredo T. J., Lust N. B., Blecic J., Stemm M., 2017, AJ, 153, 3
Delrez L., et al., 2021, Nature Astronomy, 5, 775
Duane S., Kennedy A. D., Pendleton B. J., Roweth D., 1987, Physics Letters B, 195, 216
Fei Y., Murphy C., Shibazaki Y., Shahar A., Huang H., 2016, Geophys. Res. Lett., 43, 6837
Foreman-Mackey D., 2018, Research Notes of the American Astronomical Society, 2, 31
Foreman-Mackey D., Agol E., Ambikasaran S., Angus R., 2017, AJ, 154, 220
Foreman-Mackey D., et al., 2021, arXiv e-prints, p. arXiv:2105.01994
Fulton B. J., et al., 2017, AJ, 154, 109
Gaia Collaboration et al., 2021, A&A, 649, A1
Gelman A., Rubin D. B., 1992, Statistical Science, 7, 457
Georgieva I. Y., et al., 2021, MNRAS, 505, 4684
Guerrero N. M., et al., 2021, ApJS, 254, 39
Gustafsson B., Edvardsson B., Eriksson K., Jørgensen U. G., Nordlund Å., Plez B., 2008, A&A, 486, 951
Hakim K., Rivoldini A., Van Hoolst T., Cottenier S., Jaeken J., Chust T., Steinle-Neumann G., 2018, Icarus, 313, 61
Haldemann J., Alibert Y., Mordasini C., Benz W., 2020, A&A, 643, A105
Hirano T., et al., 2018, AJ, 155, 127
Hoffman M. D., Gelman A., 2011, arXiv e-prints, p. arXiv:1111.4246
Hooton M. J., et al., 2022, A&A, 658, A75
Hoyer S., Guterman P., Demangeon O., Sousa S. G., Deleuil M., Meunier J. C., Benz W., 2020, A&A, 635, A24
Johnstone C. P., Güdel M., Brott I., Lüftinger T., 2015a, A&A, 577, A28
Johnstone C. P., et al., 2015b, ApJ, 815, L12
Kempton E. M. R., et al., 2018, PASP, 130, 114401
Kipping D. M., 2013, MNRAS, 435, 2152
Kubyshkina D., et al., 2018, A&A, 619, A151
Kubyshkina D., et al., 2019a, A&A, 632, A65
Kubyshkina D., et al., 2019b, ApJ, 879, 26
Kubyshkina D., et al., 2019c, ApJ, 879, 26
Kurucz R. L., 2013, ATLAS12: Opacity sampling model atmosphere program (ascl:1303.024)
Lacedelli G., et al., 2022, MNRAS, 511, 4551
Lam K. W. F., et al., 2021, Science, 374, 1271
Lampón M., et al., 2021, A&A, 648, L7
Leleu A., et al., 2021, A&A, 649, A26
Lendl M., et al., 2020, A&A, 643, A94
Lindegren L., et al., 2021, A&A, 649, A4
Lopez E. D., Fortney J. J., 2014, ApJ, 792, 1
Luger R., Agol E., Foreman-Mackey D., Fleming D. P., Lustig-Yaeger J., Deitrick R., 2019, AJ, 157, 64
Marigo P., et al., 2017, ApJ, 835, 77
Maxted P. F. L., et al., 2021, MNRAS,

Modirrousta-Galian D., Locci D., Micela G., 2020, ApJ, 891, 158
Morris R. L., Twicken J. D., Smith J. C., Clarke B. D., Jenkins J. M., Bryson S. T., Girouard F., Klaus T. C., 2017, Kepler Data Processing Handbook: Photometric Analysis, Kepler Science Document KSCI-19081-002
Moses J. I., et al., 2013, ApJ, 777, 34
Osborn H. P., et al., 2022, arXiv e-prints, p. arXiv:2203.03194
Persson C. M., et al., 2018, A&A, 618, A33
Piskunov N., Valenti J. A., 2017, A&A, 597, A16
Ricker G. R., et al., 2014, in Oschmann Jacobus M. J., Clampin M., Fazio G. G., MacEwen H. A., eds, Society of Photo-Optical Instrumentation Engineers (SPIE) Conference Series Vol. 9143, Space Telescopes and Instrumentation 2014: Optical, Infrared, and Millimeter Wave. p. 914320 (arXiv:1406.0151), doi:10.1117/12.2063489
Ryabchikova T., Piskunov N., Kurucz R. L., Stempels H. C., Heiter U., Pakhomov Y., Barklem P. S., 2015, Phys. Scr., 90, 054005
Salmon S. J. A. J., Van Grootel V., Buldgen G., Dupret M. A., Eggenberger P., 2021, A&A, 646, A7
Salvatier J., Wiecki T. V., Fonnesbeck C., 2016, PeerJ Computer Science, 2, e55
Schanche N., et al., 2020, MNRAS, 499, 428
Scuflaire R., Théado S., Montalbán J., Miglio A., Bourge P.-O., Godart M., Thoul A., Noels A., 2008, Ap&SS, 316, 83
Skrutskie M. F., et al., 2006, AJ, 131, 1163
Smith J. C., et al., 2012, Publ. Astron. Soc. Pac., 124, 1000
Sotin C., Grasset O., Mocquet A., 2007, Icarus, 191, 337
Stumpe M. C., et al., 2012, Publ. Astron. Soc. Pac., 124, 985
Stumpe M. C., Smith J. C., Catanzarite J. H., Van Cleve J. E., Jenkins J. M., Twicken J. D., Girouard F. R., 2014, Publ. Astron. Soc. Pac., 126, 100
Suárez Mascareño A., Rebolo R., González Hernández J. I., Esposito M., 2015, MNRAS, 452, 2745
Twicken J. D., Clarke B. D., Bryson S. T., Tenenbaum P., Wu H., Jenkins J. M., Girouard F., Klaus T. C., 2010, in Radziwill N. M., Bridger A., eds, Society of Photo-Optical Instrumentation Engineers (SPIE) Conference Series Vol. 7740, Software and Cyberinfrastructure for Astronomy. p. 774023, doi:10.1117/12.856790
Valenti J. A., Piskunov N., 1996, A&AS, 118, 595
Weiss L. M., et al., 2018a, AJ, 155, 48
Weiss L. M., et al., 2018b, AJ, 156, 254
Wilson T. G., et al., 2022, MNRAS, 511, 1043
Wright E. L., et al., 2010, AJ, 140, 1868
Yi S., Demarque P., Kim Y.-C., Lee Y.-W., Ree C. H., Lejeune T., Barnes S., 2001, ApJS, 136, 417
Zeng L., et al., 2019, Proceedings of the National Academy of Science, 116, 9723

[1] Institute of Planetary Research, German Aerospace Center (DLR), Rutherfordstrasse 2, 12489 Berlin, Germany
[2] Physikalisches Institut, University of Bern, Sidlerstrasse 5, 3012 Bern, Switzerland
[3] Cavendish Laboratory, JJ Thomson Avenue, Cambridge CB3 0HE, UK
[4] Space Research Institute, Austrian Academy of Sciences, Schmiedlstrasse 6, A-8042 Graz, Austria
[5] Observatoire Astronomique de l'Université de Genève, Chemin Pegasi 51, Versoix, Switzerland
[6] Department of Astronomy, Stockholm University, AlbaNova University Center, 10691 Stockholm, Sweden; [7] Department of Space, Earth and Environment, Chalmers University of Technology, Onsala Space Observatory, 43992 Onsala, Sweden
[8] Leiden Observatory, University of Leiden, PO Box 9513, 2300 RA Leiden, The Netherlands
[9] Aix Marseille Univ, CNRS, CNES, LAM, 38 rue Fr'ed'eric Joliot-Curie, 13388 Marseille, France
[10] Center for Space and Habitability, University of Bern, Gesellschaftsstrasse 6, 3012 Bern, Switzerland
[11] Department of Physics and Kavli Institute for Astrophysics and Space Research, Massachusetts Institute of Technology, Cambridge, MA 02139, USA
[12] Centre for Exoplanet Science, SUPA School of Physics and Astronomy, University of St Andrews, North Haugh, St Andrews KY16 9SS, UK
[13] Instituto de Astrofísica de Canarias, 38200 La Laguna, Tenerife, Spain
[14] Departamento de Astrofísica, Universidad de La Laguna, 38206 La Laguna, Tenerife, Spain
[15] Instituto de Astrofísica e Ciências do Espaço, Universidade do Porto, CAUP, Rua das Estrelas, 4150-762 Porto, Portugal
[16] Departamento de Física e Astronomia, Faculdade de Ciências, Universidade do Porto, Rua do Campo Alegre, 4169-007 Porto, Portugal
[17] Institut de Ciències de l'Espai (ICE, CSIC), Campus UAB, Can Magrans s/n, 08193 Bellaterra, Spain
[18] Institut d'Estudis Espacials de Catalunya (IEEC), 08034 Barcelona, Spain
[19] Admatis, 5. Kand'o K'alm'an Street, 3534 Miskolc, Hungary
[20] Depto. de Astrofísica, Centro de Astrobiología (CSIC-INTA), ESAC campus, 28692 Villanueva de la Cañada (Madrid), Spain
[21] Université Grenoble Alpes, CNRS, IPAG, 38000 Grenoble, France
[22] Université de Paris, Institut de physique du globe de Paris, CNRS, F-75005 Paris, France
[23] Lund Observatory, Dept. of Astronomy and Theoretical Physics, Lund University, Box 43, 22100 Lund, Sweden
[24] Astrobiology Research Unit, Université de Liège, Allée du 6 Août 19C, B-4000 Liège, Belgium
[25] Space sciences, Technologies and Astrophysics Research (STAR) Institute, Université de Liège, Allée du 6 Août 19C, 4000 Liège, Belgium
[26] Dipartimento di Fisica, Università degli Studi di Torino, via Pietro Giuria 1, I-10125, Torino, Italy
[27] Department of Astrophysics, University of Vienna, Tuerkenschanzstrasse 17, 1180 Vienna, Austria
[28] Division Technique INSU, BP 330, 83507 La Seyne cedex, France
[29] IMCCE, UMR8028 CNRS, Observatoire de Paris, PSL Univ., Sorbonne Univ., 77 av. Denfert-Rochereau, 75014 Paris, France
[30] Center for Astrophysics, Harvard & Smithsonian, 60 Garden Street, Cambridge, MA 02138, USA
[31] Institut d'astrophysique de Paris, UMR7095 CNRS, Universit'e Pierre & Marie Curie, 98bis blvd. Arago, 75014 Paris, France
[32] Department of Physics, University of Warwick, Gibbet Hill Road, Coventry CV4 7AL, United Kingdom
[33] Science and Operations Department - Science Division (SCI-SC), Directorate of Science, European Space Agency (ESA), European Space Research and Technology Centre (ESTEC), Keplerlaan 1, 2201-AZ Noordwijk, The Netherlands
[34] Konkoly Observatory, Research Centre for Astronomy and Earth Sciences, 1121 Budapest, Konkoly Thege Miklós út 15-17, Hungary
[35] ELTE Eötvös Loránd University, Institute of Physics, Pázmány Péter sétány 1/A, 1117 Budapest, Hungary
[36] Sydney Institute for Astronomy, School of Physics A29, University of Sydney, NSW 2006, Australia
[37] INAF, Osservatorio Astronomico di Padova, Vicolo dell'Osservatorio 5, 35122 Padova, Italy
[38] Astrophysics Group, Keele University, Staffordshire, ST5 5BG, United Kingdom
[39] INAF, Osservatorio Astrofisico di Catania, Via S. Sofia 78, 95123

Catania, Italy
[40] Institute of Optical Sensor Systems, German Aerospace Center (DLR), Rutherfordstrasse 2, 12489 Berlin, Germany
[41] ETH Zurich, Department of Physics, Wolfgang-Pauli-Strasse 2, CH-8093 Zurich, Switzerland
[42] Dipartimento di Fisica e Astronomia "Galileo Galilei", Universita degli Studi di Padova, Vicolo dell'Osservatorio 3, 35122 Padova, Italy [43] ESTEC, European Space Agency, 2201AZ, Noordwijk, NL
[44] Zentrum für Astronomie und Astrophysik, Technische Universität Berlin, Hardenbergstr. 36, D-10623 Berlin, Germany
[45] Institut für Geologische Wissenschaften, Freie Universität Berlin, 12249 Berlin, Germany
[46] Department of Earth, Atmospheric and Planetary Sciences, Massachusetts Institute of Technology, Cambridge, MA 02139, USA
[47] Department of Aeronautics and Astronautics, MIT, 77 Massachusetts Avenue, Cambridge, MA 02139, USA
[48] MTA-ELTE Exoplanet Research Group, 9700 Szombathely, Szent Imre h. u. 112, Hungary
[49] Institute of Astronomy, University of Cambridge, Madingley Road, Cambridge, CB3 0HA, United Kingdom
[50] Department of Astrophysical Sciences, Princeton University, 4 Ivy Ln, Princeton, NJ 08544, USA
[51] Department of Astronomy & Astrophysics, University of Chicago, Chicago, IL 60637, USA

APPENDIX A: EXTRA MATERIAL

We present in Figure A1 the posterior distribution of the fitted parameters.

This paper has been typeset from a TEX/LATEX file prepared by the author.

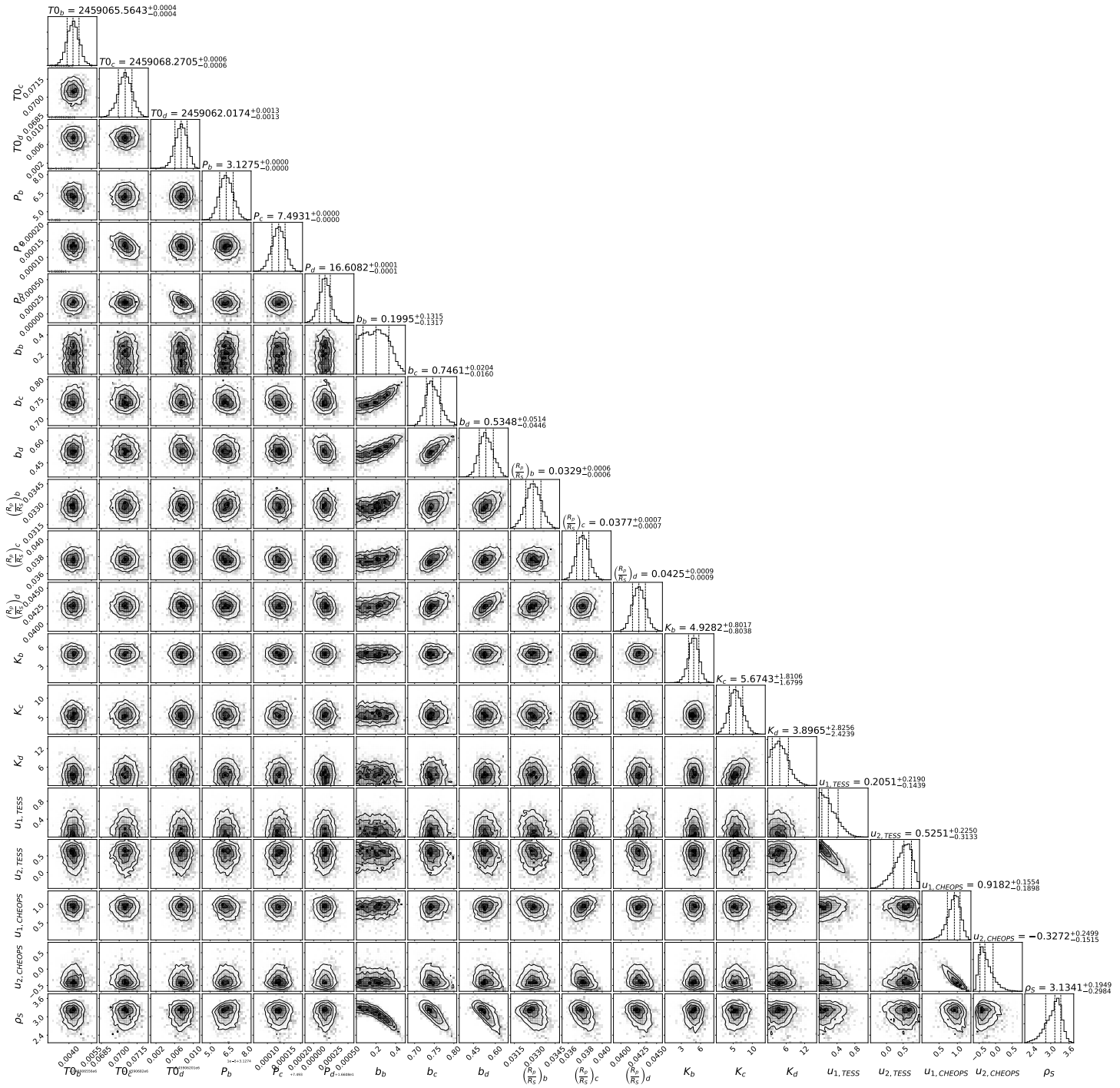

Figure A1. Corner plot showing the posterior distribution of the fitted parameters.